Multidimensional Structure Conformation of Persulfurated Benzenes for Highly Efficient Phosphorescence

Hongwei Wu,[†,‡] Glib V. Baryshnikov,[§] Artem Kuklin,[§] Boris F. Minaev,[§] Bin Wu,[⊥] Long Gu,[‡] Liangliang Zhu,[⊥] Hans Ågren,[§◊] Yanli Zhao*[‡]

[†]College of Chemistry, Chemical Engineering and Biotechnology, National Manufacturing Innovation Center of Advanced Dyeing and Finishing Technology, Donghua University, Shanghai 201620, China

[‡]Division of Chemistry and Biological Chemistry School of Physical and Mathematical Sciences Nanyang Technological University, 21 Nanyang Link, Singapore 637371.

[§]Division of Theoretical Chemistry and Biology, School of Biotechnology, KTH Royal Institute of Technology, SE-10691 Stockholm, Sweden

[⊥]State Key Laboratory of Molecular Engineering of Polymers, Department of Macromolecular Science, Fudan University, Shanghai 200433, China

[◊]Tomsk State University, 36 Lenin Avenue, 634050, Tomsk, Russian Federation

ABSTRACT: It is a challenge to acquire, realize and comprehend highly emissive phosphorescent molecules. Herein, we report that, using persulfurated benzene compounds as models, phosphorescence can be strongly enhanced through the modification of molecular conformation and crystal growth conditions. By varying the peripheral groups in these compounds, we were able to control their molecular conformation and crystal growth mode, leading to one- (1D), two- (2D) and three-dimensional (3D) crystal morphologies. Two kinds of typical molecular conformations were separately obtained in these crystals through substituent group control or solvent effect. Importantly, a symmetrical 3,3-conformer exhibits that planar central benzene ring prefers a 3D-type crystal growth mode, demonstrating high

phosphorescence efficiency. Such outcome is attributed to strong crystal protection effect of 3D crystal and bright global minimum (GM) boat-like T_1 state of the symmetrical 3,3-conformer. The conformation studies further reveal small deformation of the inner benzene ring in both singlet and triplet states. The GM boat-like T_1 state is indicated by theoretical calculations, which is far away from the conical intersection (CI) point between the S_0 and T_1 potential energy surface. Meanwhile, the small energy gap between S_1 and T_1 states and the considerable spin-orbit coupling matrix elements allow an efficient population of the T_1 state. Combined with the crystal protection and conformation effect, the 3,3-conformer crystal shows high phosphorescence efficiency. The unsymmetrical 2,4-conformer conformation with the twisted central benzene ring leads to 1D or 2D crystal growth mode, which has weak crystal protection effect. In addition, the unsymmetrical conformation has a dark GM T_1 state that is very close to the T_1-S_0 CI point, implying an efficient nonradiative T_1-S_0 quenching. Thus, weak phosphorescence was observed from the unsymmetrical conformation. This study provides an insight for the development of highly emissive phosphorescent materials.

KEYWORDS: crystal engineering • molecular conformation • persulfurated benzene • phosphorescence • supramolecular chemistry

INTRODUCTION

Organic phosphorescent materials have gained intensive attention in modern optoelectronics including light-emitting systems, luminescent displays, lasers, and bioimaging.[1-14] The past few years have witnessed substantial progress in the development of pure organic phosphorescent materials. Several strategies such as crystal engineering,[15-18] heavy atom effect,[19-21] and polymer dispersion[22-25] have been developed for inducing triplet emission. Crystal engineering is one of the most popular paths to induce phosphorescence among these strategies, because rigid crystal environments can restrict molecular vibrations and rotations to

suppress nonradiative relaxation and promote inter-system crossing (ISC).[26] Moreover, intermolecular electronic coupling in a crystal is also an important factor for phosphorescence enhancement. For example, *H*-aggregation and π-π stacking interactions can induce the emission of the triplet state in some molecular systems. However, these interactions cannot offer high phosphorescence efficiency due to the exciton energy loss during the luminescence process. As a result, most of the reported phosphorescent molecules showed the emission efficiency lower than 30%.[27] In order to enhance the phosphorescence efficiency, it is extremely important to develop a rigid crystal environment without unfavorable aggregation. However, there is still a lack of suitable models for understanding high-efficiency phosphorescence in molecular systems.

In addition to the basic factors (*i.e.*, molecular structure regularity and introduction of heavy atoms) affecting the phosphorescence efficiency, there are two additional factors that are also vital, namely molecular conformation and crystal packing. The molecular conformation has a considerable influence on the excited states of molecules and may lead to different luminous modes.[28] For example, the efficiency of delayed fluorescence and phosphorescence emissions can be affected in a different manner by tuning the conformational structures.[29] Regarding the stacking factor, the assembly mode of the crystals can significantly influence the efficiency of the molecular emission. Zhang et al. reported that coassembled crystals could show higher emission efficiency than the single molecular crystals.[30] The change of stacking direction and distance often brings different emission efficiency.[31] Therefore, tunable conformation and controlled crystal growth are crucial for understanding the phosphorescence emission efficiency of organic species.

While some multi-sulfurated aromatic compounds have been reported to show room-temperature phosphorescence in the solid state,[32,33] their emission mechanism still remains unclear due to the lack of full understanding on the crystal growth process and different

luminous efficiency among different conformations within one molecule. Hence, by controlling the two factors, the phosphorescence efficiency could be more deeply understood.[22,32] Herein, we designed and synthesized five persulfurated benzene molecules (Figure 1) by changing peripheral substituent groups on the outer six sites of the benzene ring in order to investigate the molecular conformation, assembly process and phosphorescence emission efficiency. Based on these manipulations, we can better understand the correlation between the excited state properties (*i.e.*, orbital symmetry, energy, spin-orbit coupling (SOC) strength) and the phosphorescence efficiency.

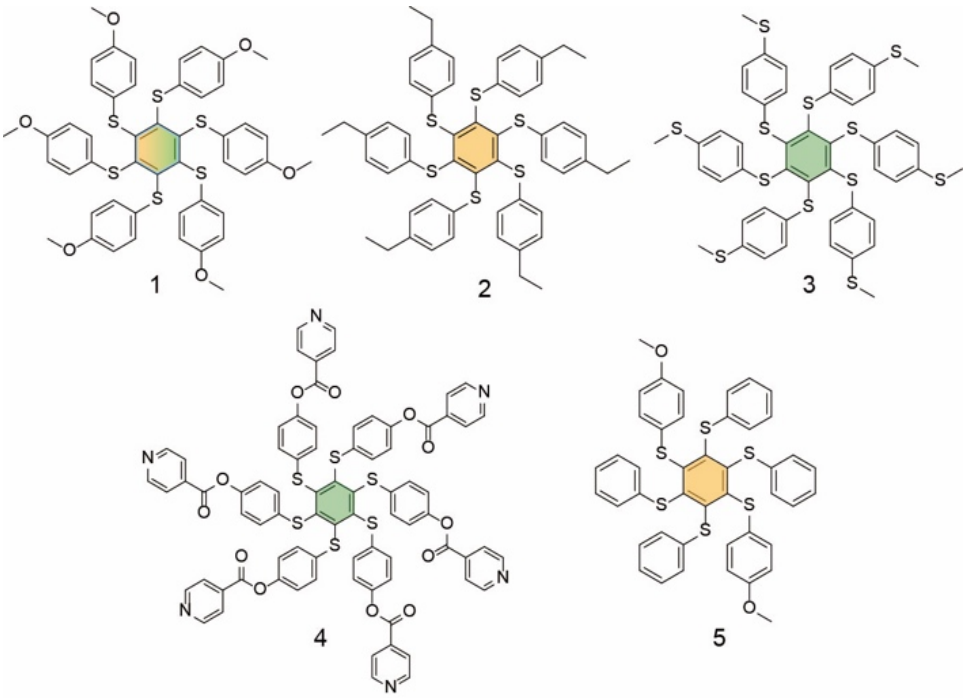

Figure 1. Chemical structures of the persulfurated benzene compounds (**1**-**5**) with different peripheral groups.

RESULTS AND DISCUSSION

The detailed synthetic protocol of the five compounds is presented in the Supporting Information. The absorbance of these compounds was recorded in *N*,*N*-dimethylformamide (DMF) and DMF with 90% water (Figure S1). Except for the intensity, no major difference of

the absorbance in DMF solution and aggregate state (DMF with 90% water) was observed. The absorption spectra in solution present a tail up to about 450 nm, which are similar to the literature report.[32,33] The emission of these persulfurated benzene compounds in DMF solution was relatively weak, while the enhanced emission was observed from the aggregate state (Figure S2). The quantum yields of these compounds in DMF with 90% water are all below 1%, showing the phosphorescence lifetime from 3 μs to 30 μs (Figure S2f). The powder state of these compounds also exhibited the phosphorescence emission (Figure S3), with higher quantum yield than corresponding aggregate state in DMF with 90% water, suggesting that the crystalline aggregation is more conducive to the phosphorescence emission. It should be noted that these compounds showed very different quantum yield values (Fig. S3d). For better understanding their photophysical properties, the crystal structures were obtained.

Compound **1** was recrystallized from various solvents and two kinds of crystal structures were obtained. Cubic crystals could be produced from ethyl acetate (defined as EA crystal), toluene mixed with isopropyl alcohol (TOU-IPR crystal), and a mixture of acetone and ethanol (ACE-ETH crystal) respectively (Figure 2a and S4 as well as Video S1), showing three-dimensional (3D) growth trend. The other type is thin lamellar crystals (Figure 2b and S4) with one-dimensional (1D) and two-dimensional (2D) features. The latter crystals were produced from chloroform mixed with isopropanol (CHL-IPR crystal), or from acetonitrile (ACN crystal). Having such a clear difference in crystal morphology, we performed single-crystal X-ray structural analysis on these crystals. The TOU-IPR, EA and ACE-ETH crystals reveal the same crystal structures (Figure 2c and S4), in which six benzene ring substituents are symmetrically distributed (3 top and 3 bottom positions) on both sides of the central benzene plane. We defined this type of structure as “3,3-conformer” for convenience. At the same time, an asymmetrical “2,4-conformer” (4 top and 2 bottom arrangements) was found from the CHL-IPR and ACN crystals (Figure 2d). The 3,3-conformer demonstrates symmetric intermolecular interactions in

six directions, where six benzene ring substituents surrounding the central benzene core have the same intermolecular orientation. Such interactions lead to a 3D type aggregation, beneficial for the formation of cubic crystals. The central benzene ring of the 3,3-conformer is more planar than that of the 2,4-conformer. For the 3,3-conformer, the dihedral angle is 0^{o} when comparing two planes of two sets of the central benzene rings (Figure 2c,d and S5). The 2,4-conformer has a large dihedral angle of 6.64^{o}. The 3D type aggregation can be explained by the stacking along two intersecting planes and the a*, b* and c* directions (Figure 2e and S5), showing a square-like frame. On the other hand, the 2,4-conformer possesses asymmetric intermolecular interactions in six directions, where the substituents connected to the central benzene core are mainly distributed in one plane (Figure 2f and S6), resulting in a dominating 1D or 2D assembly. It should be noted that the 3,3-conformer crystals tend to be formed more rapidly in high concentrations, while the 2,4-conformer crystals are more slowly formed.

To reveal the mechanisms responsible for the crystal growth, the total energy per molecule for both crystal conformations was calculated by density functional theory (DFT) within periodic boundary conditions (see Supporting Information for details). The energy minimization results reveal that both crystal structures are close in the formation energy. The 2,4-conformer is only 0.02 eV/molecule less stable than the 3,3-conformer, which is in the order of van der Waals interaction energy (Figure 2f and S7). This difference could explain more rapid formation of the 3,3-conformer in solvents. At the same time, single-molecule B3LYP/6-31G(d)[34-37] calculations predicted that the 2,4-conformer is 0.05 eV (1.3 kcal/mol) more stable than the 3,3-conformer. Without the intermolecular interactions in the crystal state, the stability of the single molecule 2,4-conformer is higher. Since both crystal conformers are energetically close to each other, their formation can be influenced by external factors, like solvent type, temperature, and pressure. These calculations suggested that the solvent may affect the crystal

growth process of compound **1**, but solvent molecules were hardly found from the crystal structures of compound **1**.

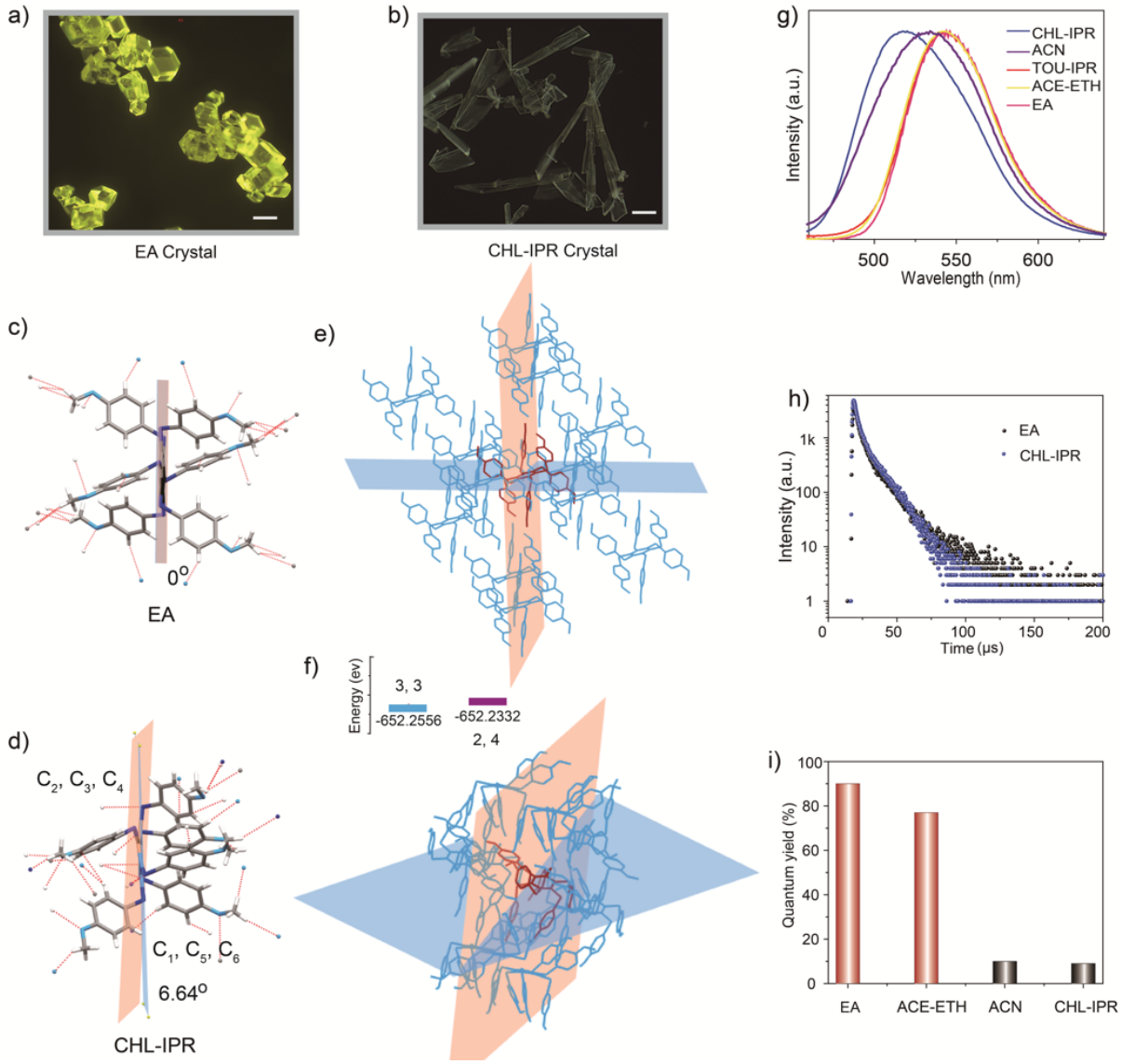

Figure 2. Crystal morphology of a) EA and b) CHL-IPR crystals of compound **1**. The scale bar is 200 μm. Molecular structures of c) EA and d) CHL-IPR crystals. e) Stacking structure of the EA crystal. f) Stacking structure of the CHL-IPR crystal, as well as calculated relative formation energy per molecule for 3,3-conformer crystal and 2,4-conformer crystal of compound **1**. Two intersecting planes are given as references, where the central benzene ring of one molecule connects neighboring molecules through intermolecular interactions. g) Stable state emission spectra of compound **1** crystals obtained in different solvents indicated. h) Phosphorescence

lifetime of EA and CHL-IPR crystals at the emission wavelength of 520 nm and 550 nm (λ_{ex} = 370 nm), respectively. i) Phosphorescent quantum yields of EA, ACE-ETH, ACN, and CHL-IPR crystals.

Concerning the emission of the obtained crystals of compound **1**, it was found that the 3,3-conformer crystals show more redshifted yellow emission as compared to that of the 2,4-conformer crystals (Figure 2g). The reason is that planar central benzene ring (Figure 2c) of the 3,3-conformer has larger conjugation degree than the twisted 2,4-conformer (Figure 2d). Meanwhile, these crystals exhibit similar phosphorescence lifetime around 1 μs (Figure 2h). In addition, the 3,3-conformer crystals present higher photoluminescence quantum yield (PLQY, about 90%) than the 2,4-conformer (around 10%, Figure 2i). Therefore, it was concluded that the crystal conformation is a crucial factor for PLQY, which can be tuned by the assembly mode related to the intermolecular interactions. The 3D type crystal morphology may provide more rigid environment for the triplet emission. In addition, the planar central benzene ring is another important factor for achieving high-efficiency phosphorescence emission.

In order to understand the relationship between the type of conformation and the para-substituents of the peripheral benzene ring, we then synthesized the molecule **2** having six ethyl groups (instead of six -OMe groups in compound **1**) at the periphery of the molecule (Figure 1). The crystals of compound **2** possess a cubic morphology with a trigonal symmetry (Figure 3a and S8) and a 3,3-conformer arrangement with the planar central benzene ring (Figure 3b and S8). The 2,4-conformer was not found from compound **2**. Six symmetrical intermolecular interactions were observed in the crystals of compound **2** (Figure 3b), where regular and symmetrical stackings were found along two intersecting planes and the a*, b* and c* three directions (Figure 3c and S9), suggesting a 3D-type aggregation.

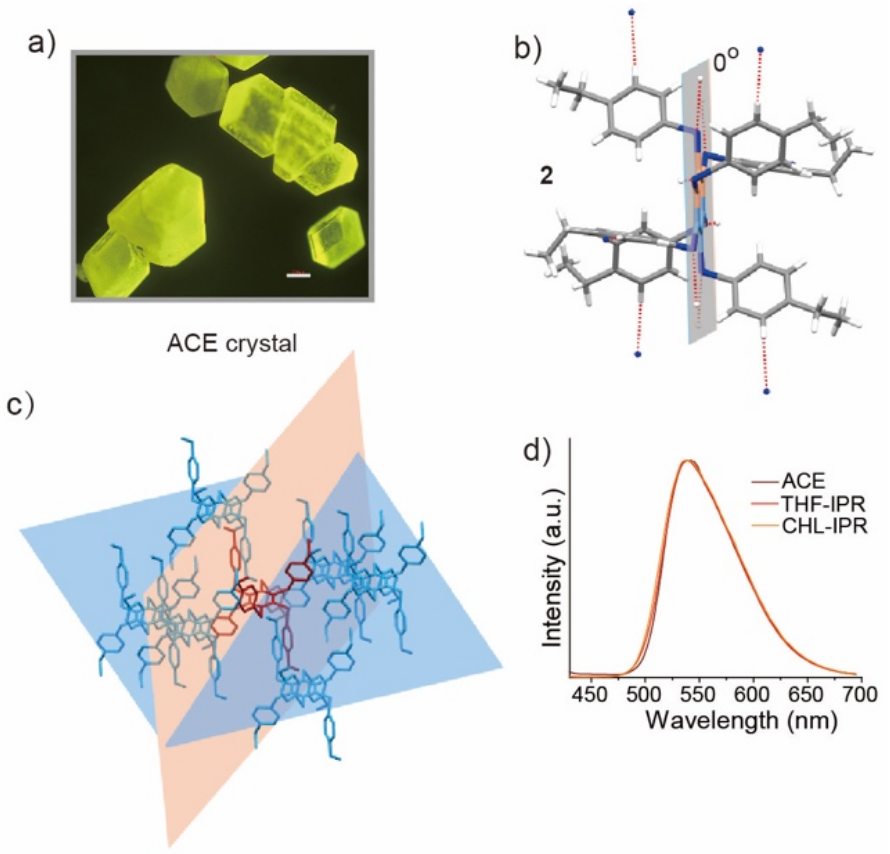

Figure 3. a) Crystal morphology and phosphorescence luminescence image of the ACE crystal of compound **2**. The scale bar is 200 μm. b) Crystal structure of the ACE crystal. c) Stacking structure of the ACE crystal by connecting the central benzene ring with neighboring molecules through intermolecular interactions and taking two intersecting planes as a reference. d) Phosphorescence spectra of ACE, THF-IPR, and CHL-IPR crystals under 365 nm excitation.

The main difference between the 3,3-conformers of compounds **1** and **2** is that the methoxy oxygen atoms could provide more interactions with neighboring molecules as compared to the -CH_2- groups. The CH_3CH_2- groups of compound **2** offer no obvious interactions, creating less steric hindrance for the 3,3-conformer arrangement. Thus, only 3,3-conformer crystals were found from compound **2**. The crystals of compound **2** obtained in different solvents show similar emission (Figure 3d), along with the phosphorescence lifetime (Figure S10) and high PLQY (around 77-85%). Combining the results of compounds **1** and **2**, it was concluded that

symmetrical 3,3-conformer with the planar central benzene ring can afford high phosphorescence efficiency more easily.

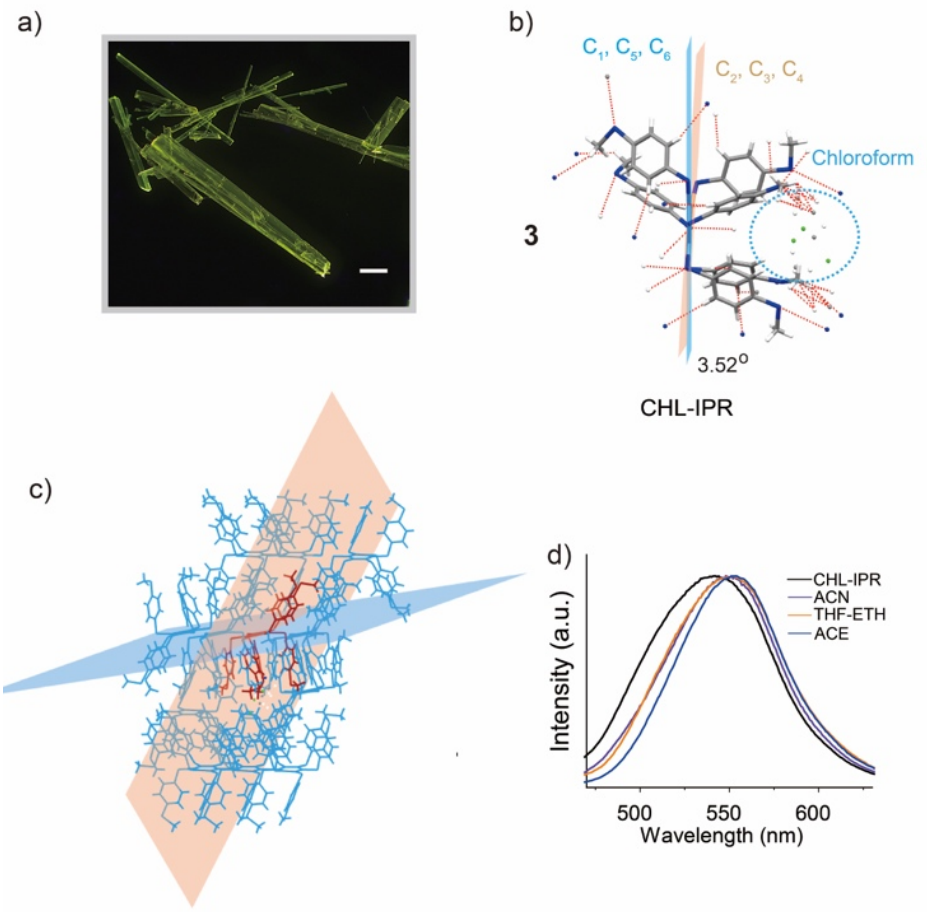

Figure 4. a) Crystal morphology and phosphorescence luminescence image of the CHL-IPR crystal of compound **3**. The scale bar is 200 μm. b) Crystal structure of the CHL-IPR crystal with twisted central benzene ring. c) Stacking structure of the CHL-IPR crystal with two intersecting planes. d) Phosphorescence spectra of CHL-IPR, ACN, THF-ETH, and ACE crystals under 365 nm excitation.

By increasing the atomic size at the six peripheral positions (-SMe instead of -OMe), we synthesized compound **3**. The crystals of compound **3** show a long thin lamellar morphology (Figure 4a and S11), which is similar to the 2,4-conformer crystal of compound **1**. The single crystal X-ray structural analysis confirms the 2,4-conformer of compound **3** with twisted central

benzene ring (Figure 4b and S12-S14). The asymmetric intermolecular interactions enable one plane to dominate the stacking interactions, like the stacking interactions in the 2,4-conformer of compound **1** (Figure 2c). The crystal structure analysis demonstrates that the sulfur atom with larger atomic radius than oxygen could interact with neighboring molecules more easily. These factors prevent the formation of the 3,3-conformer. In addition, the crystal structures of compound **3** contain solvent molecules (Figure 4b, S13 and S14), such as CHL, EA, and tetrahydrofuran (THF), in the crystalline interspace. This observation suggests that the 2,4-confomer arrangement has more intermolecular space, since the solvent molecules were not detected across the 3,3-conformer crystals of compounds **1** and **2**. Indeed, the crystallographic analysis reveals that the average volume per molecule is 817.9 and 673.8 $Å^3$ for 2,4- and 3,3-conformers of compound **1**, respectively.

The presence of different solvent molecules induces different C-S-C bond angles in compound **3** (Figure S15). These results clearly show that the solvent molecules play a crucial role and can influence the crystal growth process. Some large solvent molecules may hinder the formation of the 3,3-conformer in the case of compound **3**, because two substituents on one side of the central benzene ring in the 2,4-confomer are beneficial to free up some space to accommodate solvent molecules. In addition, solvent molecules may also interact with the edge groups (CH_3S- for compound **3**) in stabilizing the asymmetrical 2,4-conformer. In the case of compound **2** with CH_3CH_2- substituents, there is no considerable interaction with solvent molecules. The crystals of compound **3** obtained from different solvents exhibit yellow-green phosphorescence with the emission maximum in the range of 535-555 nm due to different C-S-C bond angles caused by different solvent species in the crystals (Figure 4d). The phosphorescence lifetime is almost the same among these crystals (Figure S16). The crystals exhibit low PLQY (CHL-IPR crystal: 5%; ACE crystal: 5%; ACN crystal: 11%), similar to the 2,4-conformer of compound **1** (less than 10%, Figure 2i). These results indicate that the 2,4-

conformer with twisted central benzene ring generally leads to weak phosphorescence efficiency.

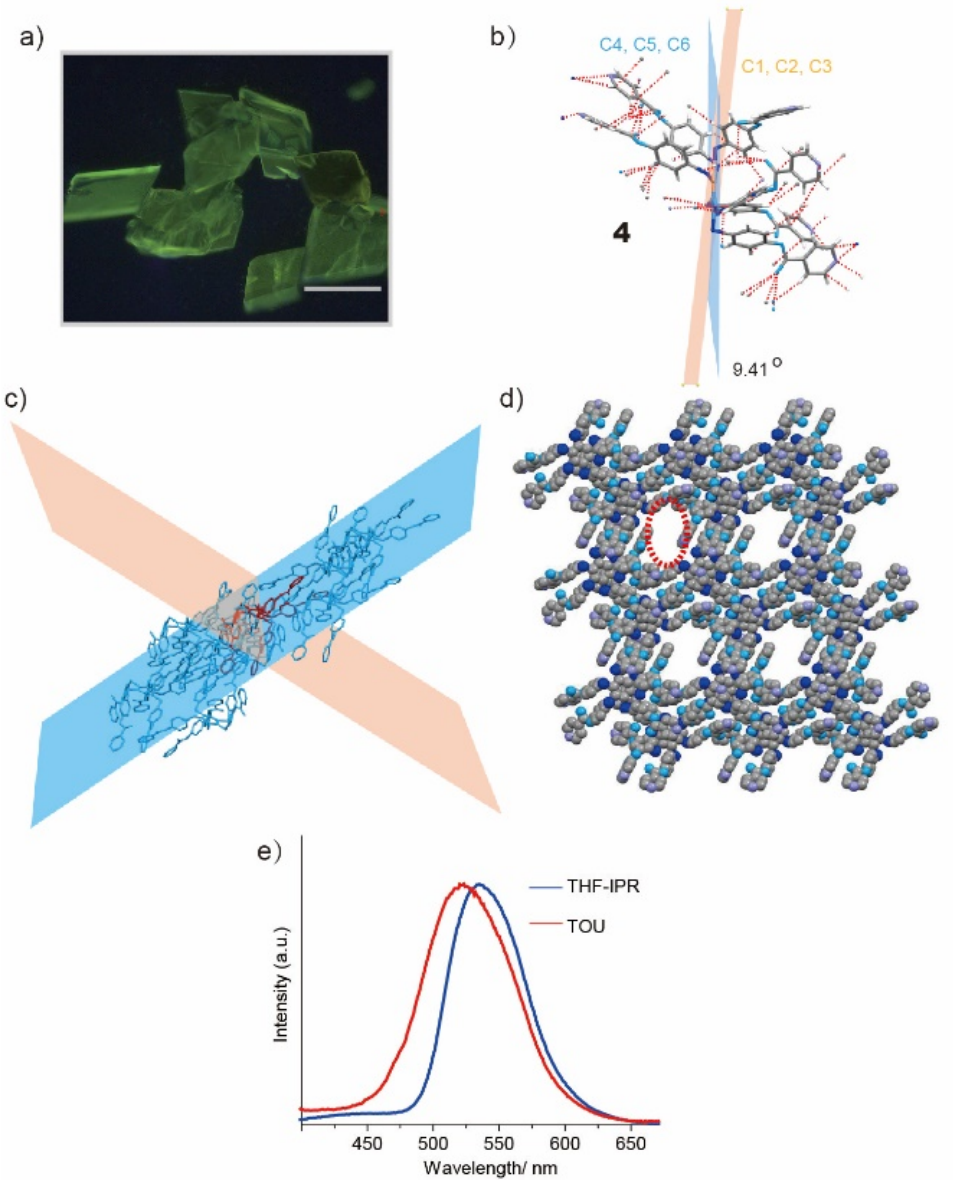

Figure 5. a) Crystal morphology and phosphorescence luminescence image of the THF-IPR crystals of compound **4**. The scale bar is 200 μm. b) Crystal structure of the THF-IPR crystals with twisted central benzene ring (dihedral angle 9.41°). c) Stacking structure of the THF-IPR crystal with two intersecting planes. d) Stacking structure of the THF-IPR crystal with 3 × 3 × 3 molecular matrix. e) Phosphorescence spectra of THF-IPR and TOU crystals under 365 nm excitation.

To more thoroughly support our conclusions, compound **4** with larger peripheral groups was synthesized. Its THF-IPR crystals show a rhombus lamellar morphology with predominated 2D growth (Figure 5a). Only the 2,4-conformer with twisted central benzene ring was observed from the crystals obtained in different solvents (Figure 5b and S17), where each molecule has asymmetrical intermolecular interactions in six directions. Solvent molecules were also found in the crystal structures due to the porous nature of the crystal packing arrangement (Figure S17). The stacking structure presents an in-plane orientation, where the central molecule connects with neighboring molecules through intermolecular interactions (Figure 5c and S18).

The 2,4-conformer formation in compound **4** should be caused by the increased size of the peripheral acetylpyridine substituents and their strong intermolecular interactions, enabling the extended self-assembly equally in two directions of one plane as compared to corresponding 2,4-conformer crystals of compounds **1** and **3**. Interestingly, a porous structure was obtained when the solvent molecules were removed (Figure 5d). The crystals of compound **4** show a green phosphorescence emission (Figure 5e). The TOU crystal shows the phosphorescence lifetime of 10.9 μs (Figure S19). The PLQY is only 2.0% and 1.8% for TOU and THF-IPR crystals, respectively. The results further indicate that the 2,4-conformer with twisted central benzene ring demonstrates weak phosphorescent emission.

Based on above results, it was concluded that the symmetrical 3,3-conformer arrangement is very important for obtaining highly efficient phosphorescence emission of persulfurated benzene compounds. However, why do the molecules only possessing the 3,3-conformer show high-efficient emission? To solve this question, we designed compound **5** with an asymmetric molecular structure (four benzene substituents and two methoxy-benzene groups located on the periphery of the central benzene ring). It was assumed that smaller substituents may allow the molecule to form the 3,3-conformer. Indeed, only the 3,3-conformer was found in crystals of

compound **5** (Figure 6a). The single crystal structural analysis demonstrates that these crystals possess asymmetric interactions due to the asymmetric structure, having a twisted central benzene ring (the dihedral angle is 21.96º when comparing two planes in central benzene ring). As a result, 1D-type crystal morphology is shown (Figure 6b and S20), where one-directional stacking is dominating (Figure 6c and S21). The crystals present orange emission (Fig 6d) with relatively low emission efficiency (around 15%) and the phosphorescence lifetime similar to compounds **1**-**4** (Figure S22). Based on these results, we can once again confirm that the symmetric 3,3-conformer with the planer central benzene ring is important for achieving highly emissive phosphorescence, since such conformation leads to strong and multi-directional crystal protection effect with respect to the phosphorescence emission. The protection effect of the 1D or 2D assembled crystals is weaker than that of the 3D one.

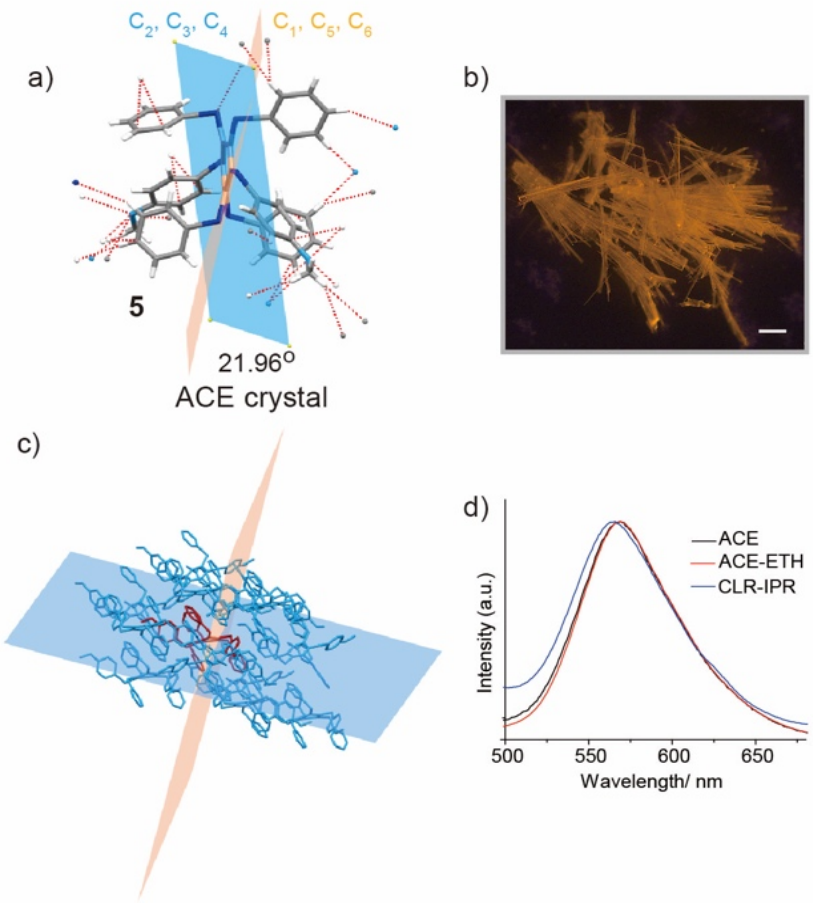

Figure 6. a) Crystal structure of the ACE crystal of compound **5**. b) Crystal morphology and phosphorescence luminescence image of the ACE crystal. The scale bar is 200 µm. c) Stacking

structure of the ACE crystal by taking two intersecting planes as a reference. d) Phosphorescence spectra of ACE, ACE-ETH, and CLR-IPR crystals under 365 nm excitation.

To understand the relationship between highly emissive phosphorescence and the conformation, we performed a series of theoretical calculations. At the initial step, we optimized the structures of the studied molecules **1**-**3** and **5** in the ground and excited states (Figure 7a, Table S1, and computational details in the Supporting Information). A clear correlation was revealed between the deformation of the central benzene ring upon triplet state excitation and the observed PLQY values. The symmetrical 3,3-conformer (EA crystal for compound **1** and CHL-IPR crystal for compound **2**) demonstrates very small torsion deformation of the central benzene ring in the ground and excited states (both T_1 and S_1), corresponding to the high PLQY for the 3,3-conformer crystals of compounds **1** and **2**. However, the 2,4-conformer for compounds **1** and **3** and unsymmetrical 3,3-conformer for compound **5** present quite high deformation of the central benzene ring in the ground S_0 state as well as in the first singlet and triplet excited states (especially in T_1 state) with small PLQY values (Figure 7a and Table S1). The reason for the phosphorescence quenching in the latter case is that the global minimum (GM) boat-like T_1 state for the unsymmetrical species is very close to the conical intersection (CI) point between the S_0 and T_1 state (Figure 7b,c) potential energy surfaces (PES). Indeed, the estimated T_1 state energy for these molecules is very small (around 0.45 eV), which implies an efficient nonradiative T_1-S_0 quenching (Figure 7b). At the same time, the local minimum (LM) of a quinoid-type T_1 state with higher excitation energy was also found (optimized) for the unsymmetrical species (Figure 7b). The excitation energy of the LM T_1 state matches well with the observed weak phosphorescence wavelength. This LM T_1 state is only 0.6 kcal mol^{-1} higher relative to the "dark" T_1 GM triplet. The barrier for the "LM T_1 to GM T_1 transition" (quinoid to boat-like transformation of the pure benzene triplet core) was also very small (less

than 1 kcal mol^{-1}),[38] meaning the presence of an efficient equilibration between the LM T_1 and GM T_1 states at room temperature (Figure 7b,c).

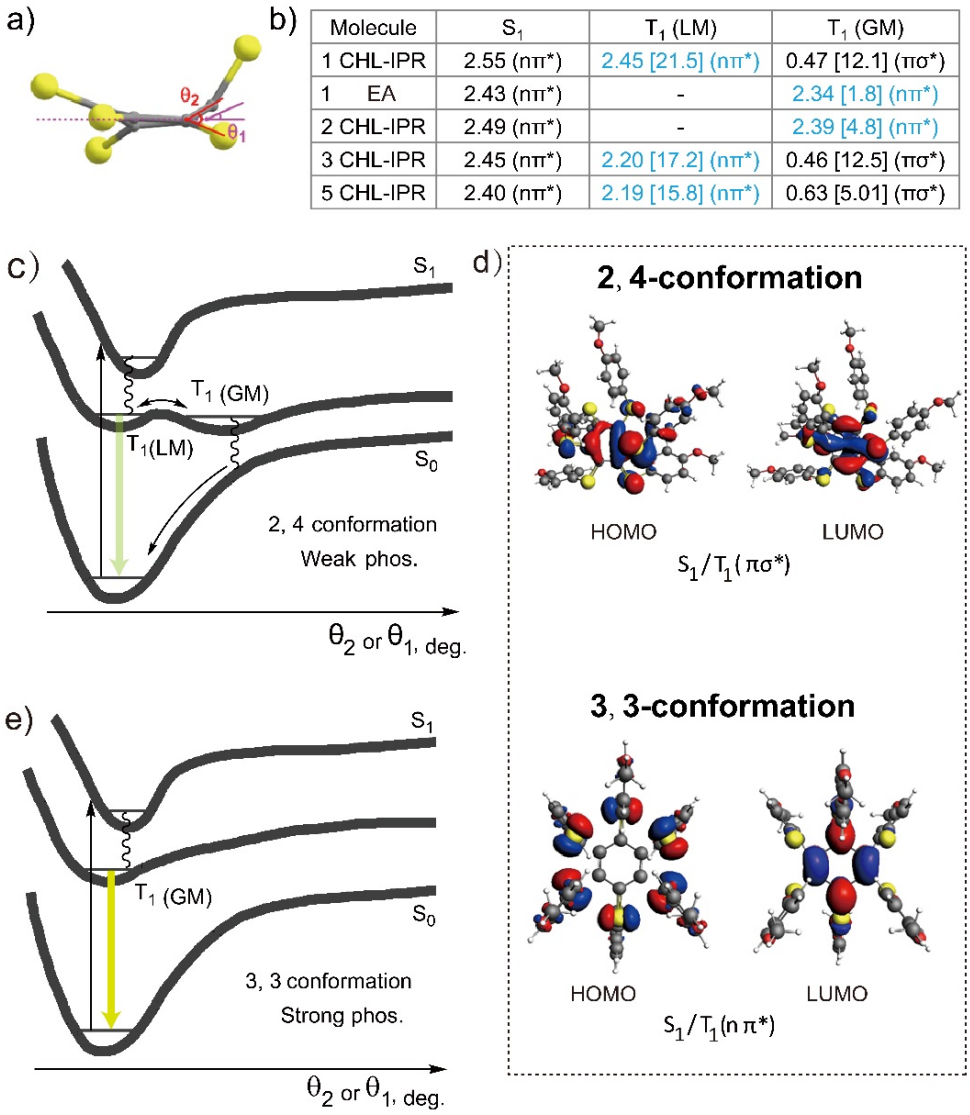

Figure 7. a) Selected dihedral angles (in deg.) that characterize the conformational structures of the central benzene ring in different electronic states. b) Calculated energy of the lowest-lying singlet (S_1) and triplet (T_1) excited states. Corresponding SOC matrix elements are presented in brackets (in cm^{-1}). For the symmetrical 3,3-conformer, the quinoid LM of T_1 state was not found. c) Qualitative representation of phosphorescence quenching through the "dark" T_1 (GM) state of πσ* nature in asymmetrically arranged 2,4-conformer of compounds **1**, **3**, and **5**. d) General view of the HOMO and LUMO wave functions for the fundamental S_1 and T_1 excited states of nπ* and πσ* symmetry (for particular compound **1** with symmetrical 3,3-

conformer and asymmetrical 2,4-conformer). e) Symmetrically arranged 3,3-conformer of compounds **1** and **2**, demonstrating strong phosphorescence from the "bright" T_1 (GM) state of nπ* nature. The wavy lines represent the nonradiative transitions between the states of different spin multiplicity promoted by the SOC effect.

It has previously been established that substituted benzene derivatives like p-dichlorbenzene possess the boat-shaped (out-of-plane distorted at one carbon atom) structure of the T_1 state.[39] Despite the πσ* nature of the boat-shaped GM T_1 state (in contrast to the LM T_1 and GM S_1 states which are of nπ* nature), the SOC between the GM S_1 and GM T_1 states of different symmetry is weaker as compared to that between the GM S_1 and LM T_1 states of the same symmetry (Figure 7b,d). The reason is the admixture of many other ππ* and πσ* configurations into the LM T_1 state (it should be mentioned that n and σ* notions here are related to the symmetry of the local moiety). Considering the strong SOC between the GM S_1 and LM T_1 states and the energy gap rule, it could be predicted that the ISC between the GM S_1 and LM T_1 states provides the main and fast deactivation channel of the excitation energy (Figure 7b,c). After the population of the LM T_1 state (Figure 7c), the equilibrium between the LM T_1 and GM T_1 states settles immediately, and the subsequent nonradiative GM T_1 relaxation into the S_0 ground state finally quenches the phosphorescence (except that a certain amount of the LM T_1 state is deactivated radiatively, giving an observable weak phosphorescence emission).

In contrast, the symmetrically arranged 3,3-conformer of compounds **1** (EA crystal) and **2** (CHL-IPR crystal) demonstrates a GM T_1 state of nπ* nature (quinoid-type structure, Figure 7b,d,e), while the boat-like structure of πσ* nature is not obtained as a stationary point on the T_1 PES in the DFT optimization (i.e., for the symmetrical 3,3-conformer arrangement relative to the central benzene ring, this πσ* T_1 state has no clear minimum on the corresponding PES).

The SOC between the S_1 and T_1 states of the same nπ* nature is quite strong (up to 4.8 cm^{-1}, Figure 7b) and the energy gap between these states is very small (about 0.1 eV), allowing efficient and fast population of T_1 state through the S_1-T_1 ISC (Figure 7b,e). As a result, compounds **1** (EA crystal) and **2** (CHL-IPR crystal) show a high triplet yield and efficient phosphorescence with high PLQY (Figure 7e). Thus, the symmetrical 3,3-conformer and asymmetrical 2,4-conformer arrangements relative to the central benzene ring in the studied compounds **1**-**3** and **5** play a key role in the deactivation pathway (emissive or nonradiative, respectively) of the excitation energy, which are in an excellent agreement with the experimental observations. It should be noted that the nonzero S_1/T_1 (nπ*) SOC is determined mostly by the sulfur atom, since the benzene ring does not contribute to the n-HOMO (Figure 7d). This is also related to the S_0/T_1 SOC and the phosphorescence radiative lifetime. Thus, the persulfurated benzene compounds are important in the search of triplet emission.

CONCLUSION

In summary, we have tuned the molecular conformation and crystal morphology through changing the peripheral substituents of asterisk-shaped persulfurated benzene compounds. The 3,3- and 2,4-conformers were obtained for this type of molecular system. The compounds with smaller peripheral substituent groups favor the 3,3-conformer formation. By having larger peripheral substituent groups, compounds show 2,4-conformer formation. Interestingly, compound **1** with the special peripheral group exhibits both 3,3- and 2,4-conformers through changing the crystallization solvents. On one hand, the symmetrical conformer arrangement could induce a 3D assembly, leading to an efficient crystal protection effect responsible for strong phosphorescence emission. On the other hand, the asymmetrical conformer with asymmetrical intermolecular interactions favors 1D or 2D crystal growth, giving weak crystal protection and therefore low phosphorescence emission. Another important factor for achieving

highly efficient phosphorescence is the planarity of the central benzene ring. The symmetrical conformer exhibits the planar central benzene ring, while the asymmetrical conformer shows the twisted central benzene ring. DFT calculations with the consideration of SOC effect show a clear correlation between the deformation of the central benzene ring upon triplet state excitation and the phosphorescence efficiency. The symmetrical conformer with small torsion deformation of the central benzene ring shows bright nπ* nature of the GM T_1 state with high PLQY. The asymmetrical conformer demonstrates quite strong deformation of the central benzene ring with the dark T_1 excited state, showing low PLQY values. By combining the crystal protection effect with the conformation effect, the factors to influence the phosphorescence efficiency of the persulfurated benzene molecules have been thoroughly understood. The present research unfolds the mechanisms of highly emissive phosphorescence through tuning the conformation of the persulfurated benzene compounds, providing a model for better understanding the phosphorescent molecular systems.

EXPERIMENTAL SECTION

Preparation for the crystals of persulfurated benzene compounds. When a mixed solvent system was used, a persulfurated benzene compound (10.0 mg) was dissolved in a good solvent (2-2.5 mL) first, and then the same amount of poor solvent was added, followed by ultrasound treatment for one minute. When a single solvent system was used, a persulfurated benzene compound (10.0 mg) was dissolved in the solvent with 3.0-5.0 mL. After the filtration, the solution was transferred into a glass vial. The glass vial was sealed by parafilm with some small holes, and placed in a quiet place. The crystals suitable for the structure analysis were formed after a few days.

ASSOCIATED CONTENT

Supporting Information. This material is available free of charge via the Internet at http://pubs.acs.org.

The synthesis, characterizations, absorption spectra, emission spectra, crystal structures and data, and phosphorescent lifetime.

Video S1: bright phosphorescence emission of 1-EA crystal under the 365 nm UV light.

Crystal cif files.

AUTHOR INFORMATION

Corresponding Author

zhaoyanli@ntu.edu.sg (Y. Z.)

ACKNOWLEDGMENT

The research is supported by the Singapore Academic Research Fund (No. RT12/19), the Singapore Agency for Science, Technology and Research (A*STAR) AME IRG grant (No. A1883c0005), the Singapore National Research Foundation Investigatorship (No. NRF-NRFI2018-03), and partially the National Key Research and Development Program of China (No. 2017YFA0207700).

REFERENCES

(1) Xu, S.; Chen, R.; Zheng, C.; Huang, W. Excited State Modulation for Organic Afterglow: Materials and Applications. *Adv. Mater*. **2016**, *28*, 9920-9940.

(2) Li, D.; Lu, F.; Wang, J.; Hu, W.; Cao, X. M.; Ma, X.; Tian, H. Amorphous Metal-Free Room-Temperature Phosphorescent Small Molecules with Multicolor Photoluminescence *via* a Host–Guest and Dual-Emission Strategy. *J. Am. Chem. Soc*. **2018**, *140*, 1916-1923.

(3) Cai, S. Z.; Shi, H.; Li, J.; Gu, L.; Ni, Y.; Cheng, Z.; Wang, S.; Xiong, W.-W.; Li, L.; An, Z.; Huang, W. Visible-Light-Excited Ultralong Organic Phosphorescence by Manipulating Intermolecular Interactions. *Adv. Mater*. **2017**, *29*, 1701244.

(4) Zhao, W.; Cheung, T. S.; Jiang, N.; Huang, W.; Lam, J. W. Y.; Zhang, X.; He, Z.; Tang, B. Z. Boosting the Efficiency of Organic Persistent Room-Temperature Phosphorescence by Intramolecular Triplet-Triplet Energy Transfer. *Nat. Commun*. **2019**, *10*, 1595.

(5) Su, Y.; Phua, S. Z. F.; Li, Y.; Zhou, X.; Jana, D.; Liu, G.; Lim, W. Q.; Ong, W. K.; Yang, C.; Zhao, Y. L. Ultralong Room Temperature Phosphorescence from Amorphous Organic Materials toward Confidential Information Encryption and Decryption. *Sci. Adv*. **2018**, *4*, eaas9732.

(6) Li, W.; Huang, Q.; Mao, Z.; Zhao, J.; Wu, H.; Chen, J.; Yang, Z.; Yang, Li, Y.; Yang, Z.; Zhang, Y.; Aldred, M.; Chi, Z. Selective Expression of Chromophores in a Single Molecule: Soft Organic Crystals Exhibiting Full-Colour Tunability and Dynamic Triplet-Exciton Behaviours. *Angew. Chem. Int. Ed*. **2020**, 59, 3739-3745.

(7) Yu, Z.; Wu, Y.; Xiao, L.; Chen, J.; Liao, Q.; Yao, J.; Fu, H. Organic Phosphorescence Nanowire Lasers. *J. Am. Chem. Soc*. **2017**, *139*, 6376-6381.

(8) He, Z.; Zhao, W.; Lam, J. W. Y.; Peng, Q.; Ma, H.; Liang, G.; Shuai, Z.; Tang, B. Z. White Light Emission from a Single Organic Molecule with Dual Phosphorescence at Room Temperature. *Nat. Commun*. **2017**, *8*, 416.

(9) Fateminia, S. A.; Mao, Z.; Xu, S.; Yang, Z.; Chi, Z.; Liu, B. Organic Nanocrystals with Bright Red Persistent Room-Temperature Phosphorescence for Biological Applications. *Angew. Chem. Int. Ed*. **2017**, *56*, 12160-12164.

(10) Wu, H.; Zhou Y.; Yin, L.; Hang, C.; Li, X.; Ågren H.; Yi, T.; Zhang, Q.; Zhu, L. Helical Self-Assembly-Induced Singlet-Triplet Emissive Switching in a Mechanically Sensitive System, *J. Am. Chem. Soc*. **2017**, *139*, 785-791.

(11) Xu, L.; Zhou, K.; Ma, H.; Lv, A.; Pei, D.; Li, G.; Zhang, Y.; An, Z.; Li, A.; He, G. Ultralong Organic Phosphorescent Nanocrystals with Long-Lived Triplet Excited States for Afterglow Imaging and Photodynamic Therapy. *ACS Appl. Mater. Interfaces* **2020**, *12*, 18385-18394.

(12) Wang, J.; Liang, J.; Xu, Y.; Liang, B.; Wei, J.; Li, C.; Mu. X.; Ye. K.; Wang, Y. Purely Organic Phosphorescence Emitter Based Efficient Electroluminescence Devices. *J. Phys. Chem. Lett*. **2019**, *10*, 5983-5988.

(13) Chen, X., Xu, C., Wang, T., Zhou, C., Du, J., Wang, Z., Xu, H.; Xie, T.; Bi, G.; Jiang, J.; Zhang, X.; Demas, J. N.; Trindle, C.; Luo, Y.; Zhang. G. Versatile Room-Temperature-Phosphorescent Materials Prepared from n-Substituted Naphthalimides: Emission Enhancement and Chemical Conjugation. *Angew. Chem. Int. Ed*. **2016**, *55*, 9872-9876.

(14) Gmelch, M.; Thomas, H.; Fries, F.; Reineke, S. Programmable Transparent Organic Luminescent Tags. *Sci. Adv*. **2019**, *5*, eaau7310.

(15) Huang, L.; Chen, B.; Zhang, X.; Trindle, C. O.; Liao, F.; Wang, Y.; Miao, H.; Luo, Y.; Zhang, G. Proton-Activated "Off-On" Room-Temperature Phosphorescence from Purely Organic Thioethers. *Angew. Chem. Int. Ed*. **2018**, *57*, 16046-16050.

(16) Shoji, Y.; Ikabata, Y.; Wang, Q.; Nemoto, D.; Sakamoto, A.; Tanaka, N.; Seino, J.; Nakai, H.; Fukushima, T. Unveiling a New Aspect of Simple Arylboronic Esters: Long-Lived Room-Temperature Phosphorescence from Heavy-Atom-Free Molecules. *J. Am. Chem. Soc*. **2017**, *139*, 2728-2733.

(17) Wang, X. F.; Xiao, H.; Chen, P. Z.; Yang, Q. Z.; Chen, B.; Tung, C. H.; Chen, Y. Z.; Wu, L. Z. Pure Organic Room Temperature Phosphorescence from Excited Dimers in Self-Assembled Nanoparticles under Visible and Near-Infrared Irradiation in Water. *J. Am. Chem. Soc*. **2019**, *141*, 5045-5050.

(18) Lucenti, E.; Forni, A.; Botta, C.; Carlucci, L.; Giannini, C.; Marinotto, D.; Pavanello, A.; Previtali, A.; Righetto, S.; Cariati, E. Cyclic Triimidazole Derivatives: Intriguing Examples of

Multiple Emissions and Ultralong Phosphorescence at Room Temperature. *Angew. Chem. Int. Ed*. **2017**, *56*, 16302-16307.

(19) An, Z.; Zheng, C.; Tao, Y.; Chen, R.; Shi, H.; Chen, T.; Wang, Z.; Li, H.; Deng, R.; Liu, X.; Huang, W. Stabilizing Triplet Excited States for Ultralong Organic Phosphorescence. *Nat. Mater*. **2015**, *14*, 685-690.

(20) Ye, W.; Wang, H.; Cai, S.; Yao, W.; Zhang, Y.; Zheng, R.; An, Z.; Huang, W. Highly Efficient Ultralong Organic Phosphorescence through Intramolecular-Space Heavy-Atom Effect. *J. Phys. Chem. Lett*. **2019**, *10*, 595-600.

(21) Wang, J., Gu, X., Ma, H., Peng, Q., Huang, X., Zheng, X., Simon H. P. Sung, Shan, G.; Lam, J.; Shuai, Z.; Tang, B. Z. A Facile Strategy for Realizing Room Temperature Phosphorescence and Single Molecule White Light Emission. *Nat. Commun*. **2018**, *9*, 2963.

(22) Wu, H.; Chi, W.; Chen, Z.; Liu, G.; Gu, L.; Bindra, A. K.; Yang, G.; Liu, X.; Zhao, Y. L. Achieving Amorphous Ultralong Room Temperature Phosphorescence by Coassembling Planar Small Organic Molecules with Polyvinyl Alcohol. *Adv. Funct. Mater*. **2019**, *29*, 1807243.

(23) Wang, S., Wu, D., Yang, S., Lin, Z., Ling, Q. Regulation of Clusterization-Triggered Phosphorescence from a Non-Conjugated Amorphous Polymer: A Platform for Colorful Afterglow. *Mater. Chem. Front*. **2020**, *4*, 1198-1205.

(24) Ma, X., Xu, C., Wang, J., Tian, H. Amorphous Pure Organic Polymers for Heavy-Atom-Free Efficient Room-Temperature Phosphorescence Emission. *Angew. Chem. Int. Ed*. **2018**, *57*, 10854-10858.

(25) Zhang, T.; Ma, X.; Wu, H.; Zhu, L.; Zhao Y.; Tian, H. Molecular Engineering for Metal-Free Amorphous Room-Temperature Phosphorescent Materials. *Angew. Chem. Int. Ed*. **2020**, *59*, 11206-11216.

(26) Yuan, W. Z.; Shen, X. Y.; Zhao, H.; Lam, J. W. Y.; Tang, L.; Lu, P.; Wang, C.; Liu, Y.; Wang, Z.; Zheng, Q.; Sun, J. Z.; Ma, Y.; Tang, B. Z. Crystallization-Induced Phosphorescence of Pure Organic Luminogens at Room Temperature. *J. Phys. Chem. C* **2010**, *114*, 6090-6099.

(27) Kenry, Chen, C.; Liu, B. Enhancing the Performance of Pure Organic Room-Temperature Phosphorescent Luminophores. *Nat. Commun*. **2019**, *10*, 2111.

(28) Data, P., Okazaki, M., Minakata, S., Takeda, Y. Thermally Activated Delayed Fluorescence *vs.* Room Temperature Phosphorescence by Conformation Control of Organic Single Molecules. *J. Mater. Chem. C* **2019**, *7*, 6616-6621.

(29) Kukhta, N. A., Huang, R., Batsanov, A. S., Bryce, M. R., Dias, F. B. Achieving Conformational Control in Room-Temperature Phosphorescence and Thermally Activated Delayed Fluorescence Emitters by Functionalization of the Central Core. *J. Phys. Chem. C* **2019**, *123*, 26536-26546.

(30) Huang, Y., Xing, J., Gong, Q., Chen, L. C., Liu, G., Yao, C., Wang, Z.; Zhang, H.; Chen, Z.; Zhang, Q. Reducing Aggregation Caused Quenching Effect through Co-Assembly of PAH Chromophores and Molecular Barriers. *Nat. Commun*. **2019**, *10*, 169.

(31) Koo, B., Swager, T. M. Highly Emissive Excimers by 2D Compression of Conjugated Polymers. *ACS Macro Lett*. **2016**, *5*, 889-893.

(32) Bergamini, G.; Fermi, A.; Botta, C.; Giovanella, U.; Motta, S. D.; Negri, F.; Peresutti, R.; Marc Gingras, M.; Ceroni. P. A Persulfurated Benzene Molecule Exhibits Outstanding Phosphorescence in Rigid Environments: From Computational Study to Organic Nanocrystals and OLED Applications. *J. Mater. Chem. C* **2013**, *1*, 2717-2724.

(33) Fermi, A.; Bergamini, G.; Peresutti, R.; Marchi, E.; Roy, M.; Ceroni, P.; Gingras, M. Molecular Asterisks with a Persulfurated Benzene Core are among the Strongest Organic Phosphorescent Emitters in the Solid State. *Dyes Pigm*. **2014**, *110*, 113-122.

(34) Hehre, W. J.; Ditchfield, R.; Pople, J. A. Self-Consistent Molecular Orbital Methods. XII. Further Extensions of Gaussian-Type Basis Sets for Use in Molecular Orbital Studies of Organic Molecules. *J. Chem. Phys*. **1972**, *56*, 2257-2261.

(35) Frisch, M. J.; Pople, J. A.; Binkley, J. S. Self-consistent Molecular Orbital Methods 25. Supplementary Functions for Gaussian Basis Sets. *J. Chem. Phys*. **1984**, *80*, 3265-3269.

(36) Becke, A. D. Density-Functional Thermochemistry. III. The Role of Exact Exchange. *J. Chem. Phys*. **1993**, *98*, 5648-5652.

(37) Lee, C.; Yang, W.; Parr, R. G. Development of the Colle-Salvetti Correlation-Energy Formula into a Functional of the Electron Density. *Phys. Rev. B* **1988**, *37*, 785–789.

(38) Zamstein, N. A Phase-Space Approach to the Radiationless Decay in Benzene: The Effect of Deuteration. *J. Chem. Phys*. **2005**, *123*, 074304.

(39) Rubio-Pons, Ò.; Minaev, B.; Loboda, O.; Hans Ågren, H. Ab Initio Calculations of Vibronic Activity in Phosphorescence Microwave Double Resonance Spectra of p-Dichlorobenzene. *Theor. Chem. Acc*. **2005**, *113*, 15-27.

Table of Contents Graphic